

## Global Warming and Drought in the 21<sup>st</sup> Century

Benjamin I Cook · Jason E Smerdon ·  
Richard Seager · Sloan Coats

Received: date / Accepted: date

**Abstract** Global warming is expected to increase the frequency and intensity of droughts in the 21<sup>st</sup> century, but the relative contributions from changes in moisture supply (precipitation) versus evaporative demand (potential evapotranspiration; PET) have not been comprehensively assessed. Using output from a suite of general circulation model (GCM) simulations from version 5 of the state-of-the-art Coupled Model Intercomparison Project (CMIP5), projected 21<sup>st</sup>-century drought trends are investigated using an offline calculated index of soil moisture balance (the Penman-Montieth based Palmer Drought Severity Index; PDSI). The PDSI calculations are used to quantify the respective contributions of precipitation and PET to projected drought trends. PDSI projections incorporating both precipitation and PET changes from the GCMs vary regionally, with robust cross-model drying in western North America, Central America, the Mediterranean, southern Africa, and the Amazon and robust wetting occurring in the Northern Hemisphere high latitudes and east Africa. These regional changes largely reflect the spatially heterogeneous response of precipitation in the models, although drying in the PDSI fields extends beyond the regions of reduced precipitation. This expansion of drought areas is attributed to globally widespread increases in PET, caused by increases in surface net radiation and the vapor pressure deficit. Increased PET not only intensifies drying in areas where precipitation is already reduced, it also drives areas into drought that would otherwise experience little drying or even wetting from precipitation trends alone. This PET amplification effect is largest

---

Benjamin I Cook  
NASA Goddard Institute for Space Studies  
2880 Broadway, New York, NY 10025  
Tel.: (212) 678-5669  
E-mail: bc9z@ldeo.columbia.edu

Jason E Smerdon  
Lamont-Doherty Earth Observatory, 61 Route 9W, Palisades, NY, 10964

Richard Seager  
Lamont-Doherty Earth Observatory, 61 Route 9W, Palisades, NY, 10964

Sloan Coats  
Lamont-Doherty Earth Observatory, 61 Route 9W, Palisades, NY, 10964

in the Northern Hemisphere mid-latitudes, and is especially pronounced in western North America, Europe, and southeast China. Compared to PDSI projections accounting for changes in precipitation only, the additional effect of increased PET expands the percentage of global land area projected to experience significant drying ( $PDSI \leq -1$ ) by the end of the 21<sup>st</sup>-century from 23% to 43%. This integrated accounting of both the supply and demand sides of the surface moisture balance is therefore critical for characterizing the full range of projected drought risks tied to increasing greenhouse gases and associated warming of the climate system.

## 1 Introduction

Extreme climate and weather events have caused significant disruptions to modern and past societies (Coumou and Rahmstorf, 2012; Ross and Lott, 2003; Lubchenco and Karl, 2012), and there is concern that anthropogenic climate change will increase the occurrence, magnitude, or impact of these events in the future (e.g., Meehl et al, 2000; Rahmstorf and Coumou, 2011). Drought is one such extreme phenomenon, and is of particular interest because of its often long-term impacts on critical water resources, agricultural production, and economic activity (e.g., Li et al, 2011; Ding et al, 2011; Ross and Lott, 2003). Focus on drought vulnerabilities has been intensified due to a series of recent and severe droughts in regions as diverse as the United States (Hoerling et al, 2012a, 2013; Karl et al, 2012), east Africa (Lyon and DeWitt, 2012), Australia (McGrath et al, 2012), and the Sahel (Giannini et al, 2003). Recent work further suggests that global aridity has increased in step with observed warming trends, and that this drying will worsen for many regions as global temperatures continue to rise with increasing anthropogenic greenhouse gas emissions (Burke et al, 2006; Dai, 2013; Sheffield and Wood, 2008).

There are significant uncertainties, however, in recent and projected future drought trends, especially regarding the extent to which these trends will be forced by changes in precipitation versus evaporative demand (also known as potential evapotranspiration; PET) (Hoerling et al, 2012b; Sheffield et al, 2012). Drought is generally defined as a deficit in soil moisture (agricultural) or streamflow (hydrologic); as such, it can be caused by declines in precipitation, increases in evapotranspiration, or a combination of the two. In the global mean, both precipitation and evapotranspiration are expected to increase with warming, a consequence of an intensified hydrologic cycle in a warmer world (Allen and Ingram, 2002; Huntington, 2006). The characteristics of changes in precipitation and PET trends at the regional level, and the dynamics that drive such changes, are nevertheless more uncertain, despite the fact that these changes are perhaps of greatest relevance to on-the-ground stakeholders.

Precipitation projections in general circulation models (GCMs) have large uncertainties compared to other model variables, such as temperature (e.g., Knutti and Sedlacek, 2013). The most confident estimates indicate that precipitation will increase in mesic areas (e.g., the wet tropics, the mid- to high latitudes of the Northern Hemisphere, etc) and decrease in semi-arid regions (e.g., the subtropics). This is generally referred to as the ‘rich-get-richer/poor-get-poorer’ mechanism, and is caused by both thermodynamic (warming and moistening of the atmosphere) and dynamic (circulation) processes (Chou et al, 2007, 2013; Held

and Soden, 2006; Neelin et al, 2003; Seager et al, 2010).

Evapotranspiration includes both the physical (evaporation) and biological (transpiration) fluxes of moisture from the surface to the atmosphere. Evapotranspiration is expected to increase in the future due to increased evaporative demand by the atmosphere, driven by increases in energy availability at the surface (surface net radiation) and vapor pressure deficits (the difference between saturation and actual vapor pressure; VPD). Increased radiative forcing from anthropogenic greenhouse gases (GHG) is expected to increase surface net radiation in most areas by inhibiting longwave cooling, while GHG-induced warming of the atmosphere is expected to increase the VPD. Importantly, VPD increases with warming, even at constant relative humidity (e.g., Anderson, 1936). Given the fact that the well-mixed nature of GHGs will drive widespread patterns of global warming, shifts in evaporative demand are likely to be more spatially homogenous and widespread than precipitation changes.

The idea that increased evaporative demand in a warmer world will enhance drought is not new (e.g., Dai, 2011), but it is important to understand where precipitation or evaporation changes will be dominant individual drivers of drought and where they will work in concert to intensify drought. To date, however, little has been done to quantify and explicitly separate the relative contribution of changes in precipitation versus evaporative demand to the magnitude and extent of global warming-induced drought. To address this question, we use output from a suite of 20<sup>th</sup> and 21<sup>st</sup>-century GCM simulations, available through the Coupled Model Intercomparison Project version 5 (CMIP5, Taylor et al, 2012) to calculate an offline index of soil moisture balance (the Penman-Monteith based Palmer Drought Severity Index). This index provides an ideal and flexible estimation of surface moisture conditions, allowing us to vary inputs such as model precipitation, temperature, and surface energy availability, which in turn allows us to separate and quantify the influence of specific variables on future drought projections. Our analysis thus addresses three questions: 1) What are the relative contributions of changes in precipitation and evaporative demand to global and regional drying patterns?, 2) Where do the combined effects of changes in precipitation and evaporative demand enhance drying?, 3) In which regions, if any, are increases in evaporative demand sufficient to shift the climate towards drought when precipitation changes would otherwise force wetter conditions?

## 2 Data and Methods

### 2.1 CMIP5 Model Output

We use GCM output available from the CMIP5 archive, the suite of model experiments organized and contributed from various modeling centers in support of the Fifth Assessment Report (AR5) of the Intergovernmental Panel on Climate Change (IPCC). Output from the historical and RCP8.5 model scenarios is used. The historical experiments are run for the years 1850–2005 and are forced with observations of transient climate forcings over the last 150 years (e.g., solar variability, land use change, GHG concentrations, etc). These experiments are initialized in 1850 using output from long, unforced control runs with fixed pre-industrial climate forcings. The RCP8.5 scenario (2006–2099) is one of a suite of

future GHG forcing scenarios; RCP8.5 is designed so that the top of the atmosphere radiative imbalance will equal approximately  $+8.5 \text{ W m}^{-2}$  by the end of the 21<sup>st</sup>-century, relative to pre-industrial conditions. The RCP8.5 scenario runs are initialized using the end of the historical runs. Our analysis is restricted to those models (Table 1) with continuous ensemble members spanning the historical through RCP8.5 time periods.

## 2.2 Penman-Monteith Palmer Drought Severity Index

Simulated soil moisture within the GCMs is not easily separated into contributions from precipitation or PET, making it difficult to identify the extent to which soil moisture trends in the models are driven by changes in supply and/or demand. Moreover, each GCM employs soil models that vary widely in their sophistication (e.g., soil depth, number of layers, etc), tunings, and parameterizations (e.g., soil texture, rooting depths, vegetation types, etc), complicating the meaningful comparison of soil moisture and drought responses across GCMs. To circumvent these issues, we use diagnostics from the GCMs to force an offline index of soil moisture balance, the Palmer Drought Severity Index (PDSI, Palmer, 1965). This flexible framework allows GCM output used in the PDSI calculation to be modified (e.g., detrended) as a means of isolating drought contributions from specific changes, such as trends in precipitation or net radiation. A common offline metric, such as PDSI, also provides a standard comparison of soil moisture balance, thus controlling for differences in soil models across the ensemble of CMIP5 GCMs.

The PDSI itself is a normalized index of drought using a simplified soil moisture balance model calculated from inputs via precipitation and losses due to evapotranspiration. PDSI is locally normalized, with negative values indicating drier than normal conditions (droughts) and positive values indicating wetter than normal conditions (pluvials), relative to a baseline calibration period for a given location. PDSI has persistence on the order of 12–18 months (Guttman, 1998; Vicente-Serrano et al, 2010), integrating moisture gains and losses throughout the calendar year, and providing a useful metric to describe longer term trends and variability in hydroclimate.

PDSI has been widely used as a metric to quantify drought in climate model simulations (e.g., Burke and Brown, 2008; Coats et al, 2013; Cook et al, 2010, 2013; Dai, 2011, 2013; Rosenzweig and Hillel, 1993; Seager et al, 2008; Taylor et al, 2013). Recent studies have highlighted some deficiencies, however, regarding the temperature-based Thornthwaite (Thornthwaite, 1948) method for estimating PET in the PDSI calculation (Dai, 2011; Hoerling et al, 2012b; Sheffield et al, 2012). The Thornthwaite method of estimating PET has the advantage of only requiring temperature data, and so has been widely used for PDSI calculations, especially over the historical period. Because Thornthwaite is largely just a linear rescaling of temperature to PET, it nevertheless significantly overestimates PET and drying in the PDSI when temperatures increase significantly beyond the mean of the baseline calibration period. This has led to several studies (e.g., Hoerling et al, 2012b; Sheffield et al, 2012) concluding that Thornthwaite based PDSI is inappropriate for use in global warming projections of drought.

Recently, there has been support for (Dai, 2013; Hoerling et al, 2012b; van der Schrier et al, 2013; Sheffield et al, 2012) the use of an alternative method for cal-

culating PET in the PDSI framework, specifically the Penman-Monteith method (Penman, 1948; Xu and Singh, 2002). Penman-Monteith is based on surface moisture and energy balance considerations (Xu and Singh, 2002), and a commonly used version is the formulation provided by the Food and Agricultural Organization (FAO) of the United Nations (Allen et al, 1998):

$$PET = \frac{0.408\Delta(R_n - G) + \gamma \frac{900}{T_a + 273} u_2 (e_s - e_a)}{\Delta + \gamma(1 + 0.34u_2)} \quad (1)$$

where PET is potential evapotranspiration ( $\text{mm day}^{-1}$ ),  $\Delta$  is the slope of the vapor pressure curve ( $\text{kPa } ^\circ\text{C}^{-1}$ ),  $R_n$  is surface net radiation ( $\text{MJ m}^{-2} \text{ day}^{-1}$ ),  $G$  is the soil heat flux density ( $\text{MJ m}^{-2} \text{ day}^{-1}$ ),  $\gamma$  is the psychrometric constant ( $\text{kPa } ^\circ\text{C}^{-1}$ ),  $T_a$  is the air temperature at 2-meters ( $^\circ\text{C}$ ),  $u_2$  is the wind speed at 2-meters ( $\text{m s}^{-1}$ ),  $e_s$  is the saturation vapor pressure (kPa), and  $e_a$  is the actual vapor pressure (kPa). The VPD is defined as  $e_s - e_a$ . Penman-Monteith based PDSI has been used, with good success, to track both observational changes in drought and changes in future drought (Dai, 2013; van der Schrier et al, 2013), and is not subject to unrealistic temperature scaling outside of the normalization interval as demonstrated for the Thornthwaite-based PDSI (Hoerling et al, 2012b; Sheffield et al, 2012). We therefore use Penman-Monteith based PDSI to quantify changes in hydroclimate for two principal reasons. First, our motivation is to analyze 21<sup>st</sup>-century projections of drought relative to a 20<sup>th</sup>-century baseline, the former of which involves temperature increases well outside the climatology of the latter. Second, the more detailed and realistic formulation of PET in the Penman-Monteith formalism allows us to separate specific variable influences on PET and therefore characterize PET-influenced droughts in terms of the net radiation and VPD changes that cause them.

### 2.3 Analyses

In the PDSI soil moisture calculation, we set the soil moisture capacities for the top and bottom layers to the standard values of 25.4 mm (1 in.) and 127 mm (5 in.). We use the 1931–1990 period from the historical runs as our baseline calibration period for the normalization. This is the same time interval used by the National Oceanographic and Atmospheric Administration for normalization of their PDSI calculations. PDSI is calculated separately for each individual ensemble member at the native resolution of the model. Diagnostics used from each GCM are monthly values of precipitation, 2-meter air temperature, surface pressure and 2-meter surface specific humidity (used to calculate vapor pressure), and surface net radiation. Ground heat flux and surface wind speed diagnostics were more difficult to obtain from these models. Relative to changes in energy availability and the VPD, Penman-Monteith PET is relatively insensitive to wind speed; we therefore set  $u_2 = 1$ . Additionally, ground heat fluxes ( $G$ ) are usually only a small fraction of the total surface energy budget, about 10–15% (Betts et al, 1996; Sellers et al, 1997). Tests in which we alternately set  $G$  to 0 or 15% of  $R_n$  indicated that the PDSI calculation is largely insensitive to this parameter. For the analyses presented herein, we therefore set  $G = 0$ .

For each continuous historical+RCP8.5 ensemble member, we calculate three

different versions of PDSI (Table 2) from 1900–2099 that serve as the basis for the majority of our analyses. PDSI-ALL references the complete PDSI calculation, incorporating changes in both precipitation and PET by using the original values of all the model variables including their trends from 1900 to 2099. In PDSI-PRE, we isolate the impact of precipitation on the PDSI calculation by detrending the temperature, vapor pressure, and net radiation variables from 2000–2099, and setting the 21<sup>st</sup>-century mean to be equal to the mean of the last two decades of the 20<sup>th</sup> century (thus retaining the variability but removing any trend from 2000–2099). In PDSI-ET, we isolate the impact of changes in evaporative demand by detrending the precipitation using an identical procedure, and retaining the transient changes in temperature, surface net radiation, and vapor pressure. We also conduct additional PDSI calculations to examine specific impacts of changes in VPD only (by detrending  $R_n$  and precipitation) and net radiation only (by detrending  $T$ , vapor pressure, and precipitation). For cross-model comparisons of PDSI and model diagnostics, all models are spatially interpolated to a common  $2^\circ \times 2^\circ$  spatial grid. For models with multiple ensemble members, the intra-model ensemble average is calculated before the multi-model ensemble average to maintain equal weighting across the 15 models. Changes in model climate variables are calculated as 2080–2099 minus 1931–1990, the same modern baseline period for the PDSI normalization.

To demonstrate the ability of PDSI to reflect changes in surface moisture balance, we calculated Pearson correlations between annual average PDSI and annual average standardized soil moisture anomalies for each grid cell for two of the models: CanESM2 and CCSM4 (Figure 1) (level by level soil moisture fields are not available from all models or ensemble members in the employed suite of CMIP5 models). Soil moisture anomalies are based on the approximate top 30 centimeters of the soil column. The correlation maps show strongly positive correlations between soil moisture and PDSI, with some isolated areas of weaker correlation. Differences between the soil moisture and PDSI fields could arise through some of the aforementioned structural differences between the GCM land surface models and the PDSI soil moisture balance model. The strong and highly positive correlations between the two estimates of moisture balance nevertheless indicate that PDSI represents well the variability in modeled surface moisture balance. This demonstration, combined with information from previous studies indicating the utility of PDSI in model applications (e.g., Burke et al, 2006; Burke and Brown, 2008; Hoerling et al, 2012b; Dai, 2011, 2013; Taylor et al, 2013), supports the use of the Penman-Monteith based PDSI for this study.

### 3 Results

#### 3.1 Model Climate Response

The forced response in surface climate from our chosen subset of CMIP5 models (Figure 2) is consistent with previous analyses of the CMIP5 climate projections (e.g., Knutti and Sedlacek, 2013). Cross-hatching in the Figure 2 panels indicates areas where at least 12 of the 15 models (80%) agree with the sign of the change in the multi-model mean. Surface net radiation increases primarily through the inhibition of longwave cooling by increased anthropogenic GHG concentrations

(Figure 2a). Land surface temperatures increase everywhere (Figure 2b), with amplified warming in the Northern Hemisphere high latitudes. Precipitation responses (Figure 2c) are spatially heterogeneous, with some regions showing drying (e.g., southwest North America, the Mediterranean, southern Africa) and others wetting (e.g., the high latitudes in the Northern Hemisphere), as per the rich-get-richer/poor-get-poorer mechanism discussed previously. Consistent with expectations, precipitation changes show much less consistency across models than the changes in surface net radiation or surface temperature. The VPD increases across all land areas (Figure 2d), primarily as a consequence of the globally widespread warming, with the largest increases occurring in regions that are projected to warm and dry (e.g., South America, southern Africa).

The models also show regional changes in summer season (JJA in the Northern Hemisphere; DJF in the Southern Hemisphere) evaporation (latent heat fluxes; Figure 2e) and in the partitioning of latent versus sensible heating (evaporative fraction or EF, Figure 2f). Evaporation (Figure 2e) increases in much of the wet tropics and the Northern Hemisphere high latitudes, where evaporative demand is enhanced (via increased VPD and surface net radiation) and precipitation generally increases. These are areas where evaporation is primarily energy (rather than moisture) limited and where evaporation continues to be energy limited in the future. In the sub-tropics, where evaporation is primarily controlled by surface moisture availability, evaporation decreases as surface moisture is unable to satisfy the increased atmospheric demand.

Changes in EF (Figure 2f), the ratio of latent heating to the sum of sensible plus latent heating, provide a diagnostic for changing moisture versus energy limitations to evaporation in the future. Areas with declining EF are regions where evaporation is increasingly moisture limited. This includes much of the sub-tropics, where evaporation is declining, but also areas of the mid-latitudes where evaporation in the future is projected to increase (e.g., central plains of North America and Europe). The fact that EF decreases in areas of both increased and decreased evaporation is suggestive of an overall decline in surface and soil moisture availability in these regions. Increases in EF are confined primarily to areas where precipitation is increasing and evaporation is limited by energy demand, such as the high northern latitudes.

### 3.2 Model PDSI Response

The efficacy of using PDSI-PRE and PDSI-ET to separate the influences of changing precipitation and evaporative demand on future drought depends on these quantities being approximately independent in their contribution to the full hydroclimate response (PDSI-ALL). While they are not likely to be completely independent, since changes in precipitation will, for many regions, affect surface radiation, temperature, and other variables, we require that to first order they sum linearly for our interpretations of precipitation and evaporative demand contributions to drought. In Figure 3, we compare PDSI-ALL to the sum of PDSI-PRE and PDSI-ET (PDSI-SUM) for each grid cell, averaged over 2080–2099. The 1:1 line, indicating a perfect match between PDSI-ALL and PDSI-SUM, is plotted as the dashed black line. PDSI-SUM and PDSI-ALL values for each model track each other closely and scatter evenly around the 1:1 line. This close match indicates

that our interpretations of PDSI-PRE and PDSI-ET as separate and additive constituents of regional drought trends are appropriate for the models and range of climate changes considered herein.

Annual average PDSI for each model and for all calculations (PDSI-ALL, PDSI-PRE, PDSI-ET) at the end of the 21<sup>st</sup> century (2080–2099) is shown in Figures 4–6. Multi-model means for these same quantities are in Figure 7; cross hatching indicates areas where the multi-model mean PDSI anomalies exceed  $-1$  or  $+1$  and where at least 12 of the 15 models also exceed these thresholds. The PDSI-ALL projection (Figure 7a) indicates substantial and robust drying over much of North America, the Amazon Basin, southern Africa, the Mediterranean, Europe, southeast China, and parts of Australia. Robust wetting occurs primarily at high latitudes in the Northern Hemisphere and east Africa. Areas of drying in PDSI-ALL generally overlap declines in EF (Figure 1f), further supporting the use of PDSI as a measure of surface moisture availability. When precipitation effects are isolated (PDSI-PRE, Figure 7b), the resulting pattern closely mirrors the changes in precipitation (Figure 1c), with substantially reduced drying in many regions relative to PDSI-ALL, especially in the mid-latitudes. These results clearly indicate that, while the global pattern of hydroclimatic change is organized around the centers of suppressed and enhanced precipitation, precipitation changes alone cannot explain the full magnitude or spatial extent of drying documented by the complete PDSI accounting. Maps of PDSI-ET (Figure 7c) demonstrate that this additional drying is the result of increased PET. Changes in PDSI-ET show nearly uniform drying of all land areas, an expected consequence of the more widespread and uniform nature of changes in surface net radiation (Figure 1a) and VPD (Figure 1d) compared to precipitation (Figure 1c). When surface net radiation and vapor deficit contributions to the drying are individually separated (Figure 8), it is clear that the relative impact of increases in the VPD is substantially larger than the effect of surface net radiation, especially in the Northern Hemisphere.

The relative impact of precipitation versus PET is further highlighted by comparing the fraction of land area (excluding Antarctica) with PDSI anomalies exceeding different drought thresholds for each of the PDSI calculations (Figure 9). For  $\text{PDSI} \leq -1$ , for example, precipitation changes alone (PDSI-PRE) cause drying on only about 23% of the global land area in the multi-model mean. Considering only increases in PET (PDSI-ET), however, leads to an equivalent magnitude of drying on nearly 70% of the global land area. For the fully simulated hydroclimate response (PDSI-ALL), the percent of land area in drought is between these two estimates, at about 43%. This reflects the fact that, depending on the region, combined PET and precipitation effects will either act to reinforce the drying ( $+PET, -precipitation$ ) or act in opposition to each other, resulting in either wetting ( $+precipitation \gg +PET$ ), drying ( $+PET \gg +precipitation$ ), or little change ( $+PET \approx +precipitation$ ).

Amplification of the drying by increases in PET is demonstrated in the zonal average PDSI from the multi-model mean (Figure 10). In PDSI-PRE (green line), nearly the entire Northern Hemisphere in the zonal mean gets wetter, with the greatest increase occurring in the high latitudes where precipitation increases are largest. PDSI-PRE changes in the mid-latitudes ( $30^\circ\text{N}$ – $50^\circ\text{N}$ ) are near neutral or slightly wetter; in these latitude bands, precipitation increases in some regions are largely counteracted by declines in other areas along this zonal band (Figure 1c). Increases in PET, reflected in PDSI-ET (red line), result in drying across all

latitudes. When both PET and precipitation are considered (PDSI-ALL, brown line), the net result is such that PET increases counter a substantial fraction of the precipitation-driven wetting in the high northern latitudes and actually push the mid-latitudes (30°N–50°N) into a drier mean state (PDSI < 0).

Four regions where the PET effects are especially pronounced are the central plains of North America (105°W–90°W, 32°N–50°N; Figure 11a), southeast China (102°E–123°E, 22°N–30°N; Figure 11b), the European-Mediterranean region (20°W–50°E, 28°N–60°N; Figure 11c), and the Amazon (70°W–45°W, 20°S–5°N Figure 11d). China and the North American central plains are especially notable because, without the effect of increased PET, these regions would be expected to stay near neutral (China, multi-model mean PDSI-PRE = +0.11), or even get wetter (North American central plains, multi-model mean PDSI-PRE = +0.63). Instead, both regions dry substantially in PDSI-ALL, shifting to a mean value of  $-1.85$  over the North American central plains and  $-1.51$  over China. In other regions, PET changes act to not only expand the spatial footprint of the regional drying, but also to amplify the changes that do occur because of reduced precipitation. In the European-Mediterranean region, PET effects intensify and expand the drying northward from the Mediterranean, shifting the regional average PDSI from  $-0.50$  (PDSI-PRE) to  $-2.53$  (PDSI-ALL). Similar intensification also happens in the Amazon, where precipitation effects result in a regional average PDSI of  $-1.40$  (PDSI-PRE), with the added effect of increased PET causing further drying in the region (PDSI-ALL =  $-3.25$ ).

#### 4 Discussion and Conclusions

Developing and refining projections of hydroclimate, drought, and water resources for the 21<sup>st</sup> century is an active area of research (e.g., Barnett and Pierce, 2009; Dai, 2013; Seager et al, 2013). To this end, significant advances have already been made in key areas, especially in our understanding of regional and seasonal precipitation responses to warming (Chou et al, 2007, 2013; Held and Soden, 2006; Neelin et al, 2003; Seager et al, 2010). Precipitation, however, does not represent the only control on ecologically and socially relevant water resources, such as streamflow, reservoir storage, and soil moisture. Evaporative demand from the atmosphere, driven by air temperature, humidity, and energy availability, can also play a critical role. It is generally accepted that a warmer world will increase evaporative demand and drying independent of precipitation changes (Dai, 2011). To date, however, few efforts have been made to explicitly separate the relative contributions to future drought trends from changes in supply (precipitation) versus demand (PET).

Using the latest suite of state-of-the-art climate model projections, we find that robust regional changes in hydroclimate are, to first order, organized around regional changes in precipitation. Increases in precipitation cause wetting in the high northern latitudes and east Africa, and precipitation declines lead to drying in the sub-tropics and Amazon. In areas where declines in precipitation already push the climate towards drought (e.g., Central America, the Amazon, southern Africa, the Mediterranean, etc), increased PET amplifies the precipitation induced drying. Critically, PET also plays a major role in enhancing drying in the midlatitudes and along the margins of the sub-tropics, where precipitation changes are small

or even positive. Globally, increased PET nearly doubles the fractional land area that will experience significant drying ( $PDSI \leq -1$ ) at the end of the 21<sup>st</sup> century, from 23% (precipitation effects only, PDSI-PRE) to 43% (precipitation+PET effects, PDSI-ALL). And in certain regions (e.g., western North America, Europe, and southeast China), PET is the sole or primary driver shifting these areas into drought. Areas dominated by the Asian monsoon (India, Indochina, etc) are some of the few places where there is little change in mean hydroclimate. In these regions, gains in moisture from increased annual and monsoon precipitation (Lee and Wang, 2012; Seo et al, 2013) are large enough to compensate for any increases in PET.

This analysis provides a comprehensive accounting of how PET and precipitation changes will each affect global hydroclimate at the end of the 21<sup>st</sup> century. For many regions, focusing on the precipitation response alone will be insufficient to fully capture changes in regional water resources such as soil moisture, runoff, or reservoir storage. Instead, increased evaporative demand will play a critical role in spreading drought beyond the sub-tropics and into the Northern Hemisphere mid-latitudes, regions of globally important agricultural production. China, for example, is the world's largest rice producer, a crop that serves as the primary nutrition source for more than 65% of the Chinese population (Peng et al, 2009). North America and much of central Asia are major centers of maize and wheat production; unlike China, they are also important exporters of these crops to the global marketplace (Headey, 2011). Increased temperatures, and the associated heat stresses, are already expected to negatively impact crop yields in these regions (Battisti and Naylor, 2009; Teixeira et al, 2013), and our analysis suggests that increases in PET due to warming and energy balance changes will have additional impacts through regional drying. Yield losses can be at least partially mitigated through management practices, such as modification of planting and harvest dates (Deryng et al, 2011). However, recent research suggests that climate change over the last 20 years is already having a deleterious impact on agricultural production (Lobell et al, 2011), and the ability of existing water resources to keep pace with future climate impacts is in question (Wada et al, 2013; Zhang et al, 2013). Even with pro-active management, our results suggest increased drought, driven primarily by increases in PET, will likely have significant ramifications for globally important regions of agricultural production in the Northern Hemisphere mid-latitudes.

**Acknowledgements** We acknowledge the World Climate Research Programme's Working Group on Coupled Modelling, which is responsible for CMIP, and we thank the climate modeling groups (listed in Table 1 of this paper) for producing and making available their model output. For CMIP, the U.S. Department of Energy's Program for Climate Model Diagnosis and Intercomparison provides coordinating support and led development of software infrastructure in partnership with the Global Organization for Earth System Science Portals. RS and JES were supported in part by the NOAA award Global Decadal Hydroclimate Variability and Change (NA10OAR431037). RS was also supported by NSF award ATM09-02716 and NOAA award NA08-OAR4320912. BIC was supported by NASA. LDEO Publication number #.

## References

- Allen MR, Ingram WJ (2002) Constraints on future changes in climate and the hydrologic cycle. *Nature* 419(6903):224–232, DOI <http://dx.doi.org/10.1038/nature01092>
- Allen RG, Pereira LS, Raes D, Smith M, et al (1998) Crop Evapotranspiration-Guidelines for Computing Crop Water Requirements. FAO Irrigation and Drainage Paper 56
- Anderson DB (1936) Relative humidity or vapor pressure deficit. *Ecology* 17(2):277–282
- Barnett TP, Pierce DW (2009) Sustainable water deliveries from the Colorado River in a changing climate. *Proceedings of the National Academy of Sciences* 106(18):7334–7338, DOI 10.1073/pnas.0812762106
- Battisti DS, Naylor RL (2009) Historical Warnings of Future Food Insecurity with Unprecedented Seasonal Heat. *Science* 323(5911):240–244, DOI 10.1126/science.1164363
- Betts AK, Ball JH, Beljaars ACM, Miller MJ, Viterbo PA (1996) The land surface-atmosphere interaction: A review based on observational and global modeling perspectives. *Journal of Geophysical Research: Atmospheres* 101(D3):7209–7225, DOI 10.1029/95JD02135
- Burke EJ, Brown SJ (2008) Evaluating Uncertainties in the Projection of Future Drought. *Journal of Hydrometeorology* 9(2):292–299, DOI 10.1175/2007JHM929.1
- Burke EJ, Brown SJ, Christidis N (2006) Modeling the recent evolution of global drought and projections for the twenty-first century with the Hadley Centre climate model. *Journal of Hydrometeorology* 7(5):1113–1125, DOI <http://dx.doi.org/10.1175/JHM544.1>
- Chou C, Tu JY, Tan PH (2007) Asymmetry of tropical precipitation change under global warming. *Geophysical Research Letters* 34(17), DOI 10.1029/2007GL030327
- Chou C, Chiang JCH, Lan CW, Chung CH, Liao YC, Lee CJ (2013) Increase in the range between wet and dry season precipitation. *Nature Geoscience* 6(4):263–267, DOI <http://dx.doi.org/10.1038/ngeo1744>
- Coats S, Smerdon JE, Seager R, Cook BI, González-Rouco JF (2013) Megadroughts in Southwestern North America in ECHO-G. *Journal of Climate* e-View, DOI doi: 10.1175/JCLI-D-12-00603.1
- Cook BI, Seager R, Miller RL, Mason JA (2013) Intensification of North American megadroughts through surface and dust aerosol forcing. *Journal of Climate* 26:4414–4430, DOI <http://dx.doi.org/10.1175/JCLI-D-12-00022.1>
- Cook ER, Seager R, Heim Jr RR, Vose RS, Herweijer C, Woodhouse C (2010) Megadroughts in North America: placing IPCC projections of hydroclimatic change in a long-term palaeoclimate context. *Journal of Quaternary Science* 25(1):48–61, DOI 10.1002/jqs.1303
- Coumou D, Rahmstorf S (2012) A decade of weather extremes. *Nature Climate Change* 2(7):491–496, DOI 10.1038/nclimate1452
- Dai A (2011) Drought under global warming: a review. *Wiley Interdisciplinary Reviews: Climate Change* 2(1):45–65, DOI 10.1002/wcc.81
- Dai A (2013) Increasing drought under global warming in observations and models. *Nature Climate Change* 3(1):52–58, DOI 10.1038/nclimate1633

- Deryng D, Sacks WJ, Barford CC, Ramankutty N (2011) Simulating the effects of climate and agricultural management practices on global crop yield. *Global Biogeochemical Cycles* 25(2), DOI 10.1029/2009GB003765
- Ding Y, Hayes MJ, Widhalm M (2011) Measuring economic impacts of drought: a review and discussion. *Disaster Prevention and Management* 20(4):434–446, DOI 10.1108/09653561111161752
- Giannini A, Saravanan R, Chang P (2003) Oceanic Forcing of Sahel Rainfall on Interannual to Interdecadal Time Scales. *Science* 302(5647):1027–1030, DOI 10.1126/science.1089357
- Guttman NB (1998) Comparing the Palmer Drought Index and the Standardized Precipitation Index. *Journal of the American Water Resources Association* 34:113–121, DOI 10.1111/j.1752-1688.1998.tb05964.x
- Headey D (2011) Rethinking the global food crisis: The role of trade shocks. *Food Policy* 36(2):136 – 146, DOI <http://dx.doi.org/10.1016/j.foodpol.2010.10.003>
- Held I, Soden B (2006) Robust responses of the hydrological cycle to global warming. *Journal of Climate* 19(21):5686–5699, DOI <http://dx.doi.org/10.1175/JCLI3990.1>
- Hoerling M, Kumar A, Dole R, Nielsen-Gammon JW, Eischeid J, Perlwitz J, Quan XW, Zhang T, Pegion P, Chen M (2012a) Anatomy of an Extreme Event. *Journal of Climate* 26(9):2811–2832, DOI 10.1175/JCLI-D-12-00270.1
- Hoerling M, Eischeid J, Kumar A, Leung R, Mariotti A, Mo K, Schubert S, Seager R (2013) Causes and Predictability of the 2012 Great Plains Drought. *Bulletin of the American Meteorological Society* in press
- Hoerling MP, Eischeid JK, Quan XW, Diaz HF, Webb RS, Dole RM, Easterling DR (2012b) Is a Transition to Semipermanent Drought Conditions Imminent in the U.S. Great Plains? *Journal of Climate* 25(24):8380–8386, DOI 10.1175/JCLI-D-12-00449.1
- Huntington TG (2006) Evidence for intensification of the global water cycle: Review and synthesis. *Journal of Hydrology* 319(1–4):83–95, DOI <http://dx.doi.org/10.1016/j.jhydrol.2005.07.003>
- Karl TR, Gleason BE, Menne MJ, McMahon JR, Heim RR, Brewer MJ, Kunkel KE, Arndt DS, Privette JL, Bates JJ, Groisman PY, Easterling DR (2012) U.S. temperature and drought: Recent anomalies and trends. *EOS, Transactions of the American Geophysical Union* 93(47):473–474, DOI 10.1029/2012EO470001
- Knutti R, Sedlacek J (2013) Robustness and uncertainties in the new CMIP5 climate model projections. *Nature Climate Change* 3(4):369–373, DOI 10.1038/nclimate1716
- Lee JY, Wang B (2012) Future change of global monsoon in the CMIP5. *Climate Dynamics* pp 1–19, DOI 10.1007/s00382-012-1564-0
- Li X, Waddington SR, Dixon J, Joshi AK, Vicente MC (2011) The relative importance of drought and other water-related constraints for major food crops in South Asian farming systems. *Food Security* 3(1):19–33, DOI 10.1007/s12571-011-0111-x
- Lobell DB, Schlenker W, Costa-Roberts J (2011) Climate Trends and Global Crop Production Since 1980. *Science* 333(6042):616–620, DOI 10.1126/science.1204531
- Lubchenco J, Karl TR (2012) Predicting and managing extreme weather events. *Physics Today* 65(3):31, DOI <http://dx.doi.org/10.1063/PT.3.1475>

- Lyon B, DeWitt DG (2012) A recent and abrupt decline in the East African long rains. *Geophysical Research Letters* 39(2):L02,702, DOI 10.1029/2011GL050337
- McGrath GS, Sadler R, Fleming K, Tregoning P, Hinz C, Veneklaas EJ (2012) Tropical cyclones and the ecohydrology of Australia's recent continental-scale drought. *Geophysical Research Letters* 39(3), DOI 10.1029/2011GL050263
- Meehl GA, Zwiers F, Evans J, Knutson T, Mearns L, Whetton P (2000) Trends in Extreme Weather and Climate Events: Issues Related to Modeling Extremes in Projections of Future Climate Change\*. *Bulletin of the American Meteorological Society* 81(3):427–436, DOI 10.1175/1520-0477(2000)081<0427:TIEWAC>2.3.CO;2
- Neelin JD, Chou C, Su H (2003) Tropical drought regions in global warming and El Niño teleconnections. *Geophysical Research Letters* 30(24), DOI 10.1029/2003GL018625
- Palmer W (1965) Meteorological drought. Research paper 45:1–58
- Peng S, Tang Q, Zou Y (2009) Current Status and Challenges of Rice Production in China. *Plant Production Science* 12(1):3–8, DOI <http://dx.doi.org/10.1626/pps.12.3>
- Penman HL (1948) Natural Evaporation from Open Water, Bare Soil and Grass. *Proceedings of the Royal Society of London Series A Mathematical and Physical Sciences* 193(1032):120–145
- Rahmstorf S, Coumou D (2011) Increase of extreme events in a warming world. *Proceedings of the National Academy of Sciences* 108(44):17,905–17,909, DOI 10.1073/pnas.1101766108
- Rosenzweig C, Hillel D (1993) The dust bowl of the 1930s: Analog of greenhouse effect in the Great Plains? *Journal of Environmental Quality* 22(1):9–22
- Ross TF, Lott N (2003) A climatology of 1980-2003 extreme weather and climate events. Tech. rep., NOAA/NESDIS. National Climatic Data Center, Asheville, NC.
- van der Schrier G, Barichivich J, Briffa KR, Jones PD (2013) A scPDSI-based global data set of dry and wet spells for 1901–2009. *Journal of Geophysical Research: Atmospheres* DOI 10.1002/jgrd.50355
- Seager R, Burgman R, Kushnir Y, Clement A, Cook E, Naik N, Miller J (2008) Tropical Pacific forcing of North American Medieval Megadroughts: Testing the Concept with an Atmosphere Model Forced by Coral-Reconstructed SSTs. *Journal of Climate* 21(23):6175–6190, DOI <http://dx.doi.org/10.1175/2008JCLI2170.1>
- Seager R, Naik N, Vecchi GA (2010) Thermodynamic and Dynamic Mechanisms for Large-Scale Changes in the Hydrological Cycle in Response to Global Warming. *Journal of Climate* 23(17):4651–4668, DOI 10.1175/2010JCLI3655.1
- Seager R, Ting M, Li C, Naik N, Cook B, Nakamura J, Liu H (2013) Projections of declining surface-water availability for the southwestern United States. *Nature Climate Change* 3:482–486, DOI 10.1038/nclimate1787
- Sellers PJ, Dickinson RE, Randall DA, Betts AK, Hall FG, Berry JA, Collatz GJ, Denning AS, Mooney HA, Nobre CA, Sato N, Field CB, Henderson-Sellers A (1997) Modeling the Exchanges of Energy, Water, and Carbon Between Continents and the Atmosphere. *Science* 275(5299):502–509, DOI 10.1126/science.275.5299.502
- Seo KH, Ok J, Son JH, Cha DH (2013) Assessing future changes in the East Asian summer monsoon using CMIP5 coupled models. *Journal of Climate* DOI

- 10.1175/JCLI-D-12-00694.1
- Sheffield J, Wood EF (2008) Projected changes in drought occurrence under future global warming from multi-model, multi-scenario, IPCC AR4 simulations. *Climate Dynamics* 31(1):79–105, DOI 10.1007/s00382-007-0340-z
- Sheffield J, Wood EF, Roderick ML (2012) Little change in global drought over the past 60 years. *Nature* 491(7424):435–438, DOI 10.1038/nature11575
- Taylor IH, Burke E, McColl L, Falloon PD, Harris GR, McNeall D (2013) The impact of climate mitigation on projections of future drought. *Hydrology and Earth System Sciences* 17(6):2339–2358, DOI 10.5194/hess-17-2339-2013
- Taylor KE, Stouffer RJ, Meehl GA (2012) An Overview Of CMIP5 And The Experiment Design. *Bulletin of the American Meteorological Society* 93(4):485–498, DOI <http://dx.doi.org/10.1175/BAMS-D-11-00094.1>
- Teixeira EI, Fischer G, van Velthuisen H, Walter C, Ewert F (2013) Global hot-spots of heat stress on agricultural crops due to climate change. *Agricultural and Forest Meteorology* 170(0):206–215, DOI <http://dx.doi.org/10.1016/j.agrformet.2011.09.002>
- Thornthwaite C (1948) An approach toward a rational classification of climate. *Geographical review* 38(1):55–94
- Vicente-Serrano SM, Beguería S, López-Moreno JI, Angulo M, El Kenawy A (2010) A new global 0.5 gridded dataset (1901-2006) of a multiscalar drought index: comparison with current drought index datasets based on the Palmer Drought Severity Index. *Journal of Hydrometeorology* 11(4):1033–1043, DOI <http://dx.doi.org/10.1175/2010JHM1224.1>
- Wada Y, Wisser D, Eisner S, Flörke M, Gerten D, Haddeland I, Hanasaki N, Masaki Y, Portmann FT, Stacke T, Tessler Z, Schewe J (2013) Multi-model projections and uncertainties of irrigation water demand under climate change. *Geophysical Research Letters* DOI 10.1002/grl.50686
- Xu CY, Singh VP (2002) Cross Comparison of Empirical Equations for Calculating Potential Evapotranspiration with Data from Switzerland. *Water Resources Management* 16(3):197–219, DOI 10.1023/A:1020282515975
- Zhang T, Simelton E, Huang Y, Shi Y (2013) A Bayesian assessment of the current irrigation water supplies capacity under projected droughts for the 2030s in China. *Agricultural and Forest Meteorology* 178–179(0):56 – 65, DOI [dx.doi.org/10.1016/j.agrformet.2012.06.002](http://dx.doi.org/10.1016/j.agrformet.2012.06.002)

**Table 1** Continuous model ensembles from the CMIP5 experiments (historical+RCP8.5) used in this analysis, including the modeling center or group that supplied the output, the number of ensemble members that met our criteria for inclusion, and the approximate spatial resolution.

Model	Modeling Center (or Group)	# Runs	Lat/Lon Resolution
CanESM2	CCCMA <sup>a</sup>	5	2.8°x2.8°
CCSM4	NCAR <sup>b</sup>	6	0.94°x1.25°
CNRM-CM5	CNRM-CERFACS <sup>c</sup>	4	1.4°x1.4°
CSIRO-MK3.6.0	CSIRO-QCCCE <sup>d</sup>	5	1.87°x1.87°
GFDL-CM3	NOAA GFDL <sup>e</sup>	1	2.0°x2.5°
GFDL-ESM2G	NOAA GFDL <sup>e</sup>	1	2.0°x2.5°
GFDL-ESM2M	NOAA GFDL <sup>e</sup>	1	2.0°x2.5°
GISS-E2-R	NASA GISS <sup>f</sup>	1	2.0°x2.5°
INMCM4.0	INM <sup>g</sup>	1	1.5°x2.0°
IPSL-CM5A-LR	IPSL <sup>h</sup>	4	1.9°x3.75°
MIROC5	MIROC <sup>i</sup>	1	1.4°x1.4°
MIROC-ESM	MIROC <sup>j</sup>	1	2.8°x2.8°
MIROC-ESM-CHEM	MIROC <sup>j</sup>	1	2.8°x2.8°
MRI-CGCM3	MRI <sup>k</sup>	1	1.1°x1.1°
NorESM1-M	NCC <sup>l</sup>	1	1.9°x2.5°

<sup>a</sup>Canadian Centre for Climate Modelling and Analysis

<sup>b</sup>National Center for Atmospheric Research

<sup>c</sup>Centre National de Recherches Météorologiques / Centre Européen de Recherche et Formation Avancée en Calcul Scientifique

<sup>d</sup>Commonwealth Scientific and Industrial Research Organization in collaboration with Queensland Climate Change Centre of Excellence

<sup>e</sup>NOAA Geophysical Fluid Dynamics Laboratory

<sup>f</sup>NASA Goddard Institute for Space Studies

<sup>g</sup>Institute for Numerical Mathematics

<sup>h</sup>Institut Pierre-Simon Laplace

<sup>i</sup>Atmosphere and Ocean Research Institute (The University of Tokyo), National Institute for Environmental Studies, and Japan Agency for Marine-Earth Science and Technology

<sup>j</sup>Japan Agency for Marine-Earth Science and Technology, Atmosphere and Ocean Research Institute (The University of Tokyo), and National Institute for Environmental Studies

<sup>k</sup>Meteorological Research Institute

<sup>l</sup>Norwegian Climate Centre

**Table 2** Description of different versions of the PDSI calculations, and the model diagnostics used in their calculation. Variables are: tsurf (2-meter surface air temperature), prec (precipitation), q (specific humidity), and rnet (surface net radiation). Detrended variables have the trend from 2000–2099 removed and replaced with mean conditions for 1980–1999.

PDSI	Transient Variables	Detrended Variables
PDSI-ALL	tsurf, prec, q, rnet	none
PDSI-PRE	prec	tsurf, q, rnet
PDSI-ET	tsurf, q, rnet	prec

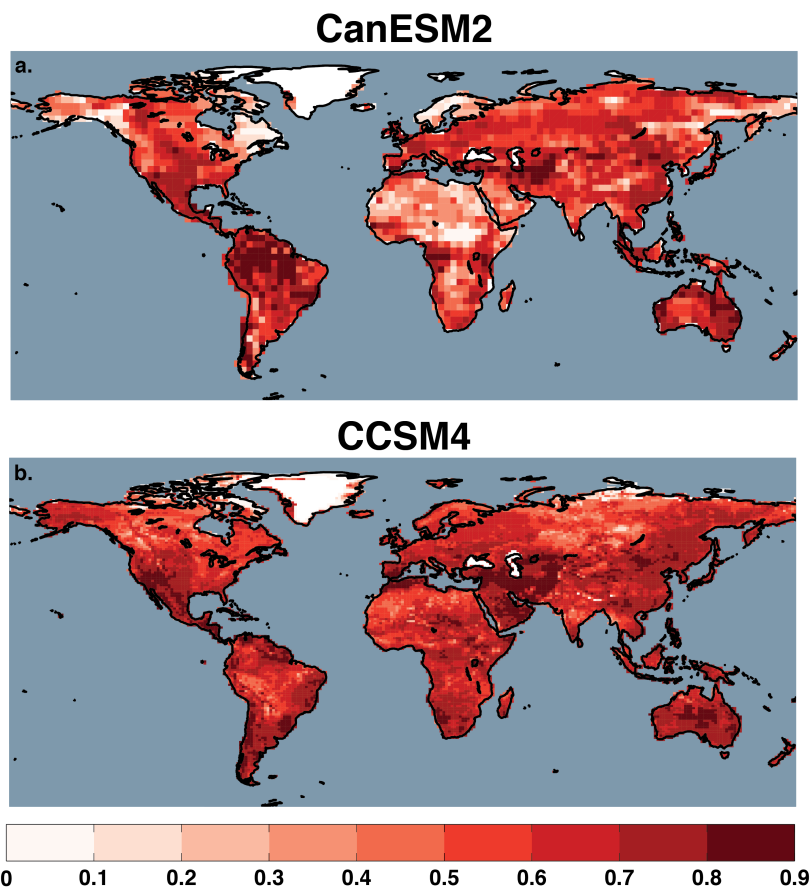


**Fig. 1** Pearson's correlation coefficients calculated between PDSI and annual average model soil moisture from the approximate top 30 centimeters of the soil column: CanESM2 (a) and CCSM4 (b). Maps represent average correlations across a five member ensemble for each model; the comparison interval is 1901-2099.

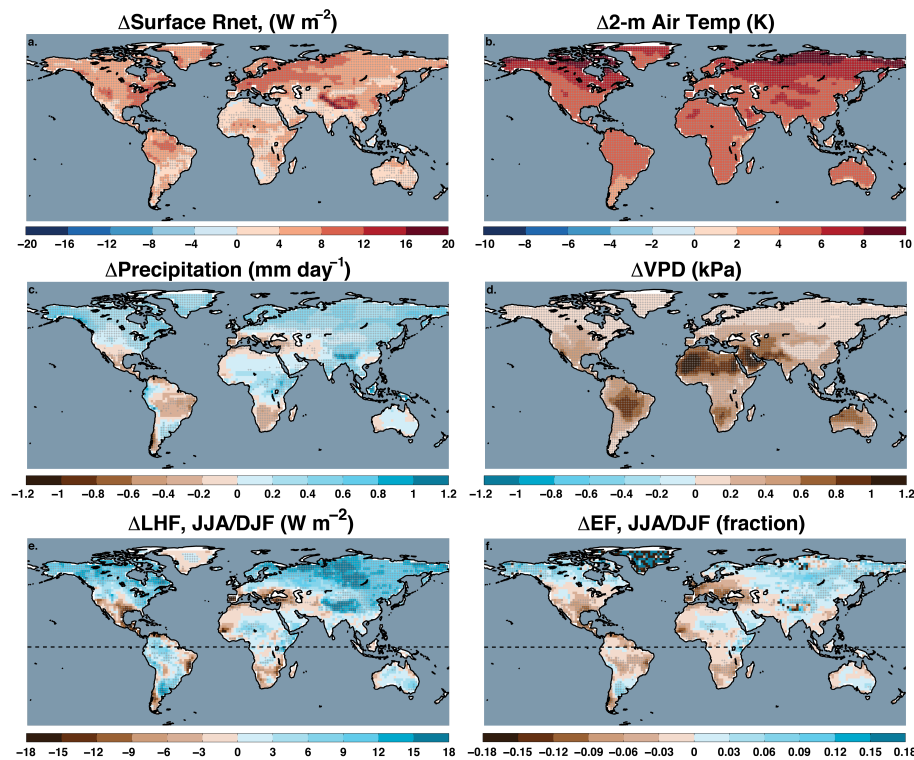


**Fig. 2** Multi-model mean changes (2080–2099 minus 1931–1990) in a) surface net radiation ( $\text{W m}^{-2}$ ), b) 2-meter air temperature (K), c) precipitation ( $\text{mm day}^{-1}$ ), d) vapor pressure deficit (kPa), e) latent heat fluxes ( $\text{W m}^{-2}$ ), and f) evaporative fraction (fraction). Panels a)–d) are annual averages. In e)–f), averages north of the equator (the dashed line) are for boreal summer (June–July–August) and south of the equator are for austral summer (December–January–February). Cross hatching indicates areas where the sign of change in at least 12 of the 15 models agrees with the sign of the multi-model mean.

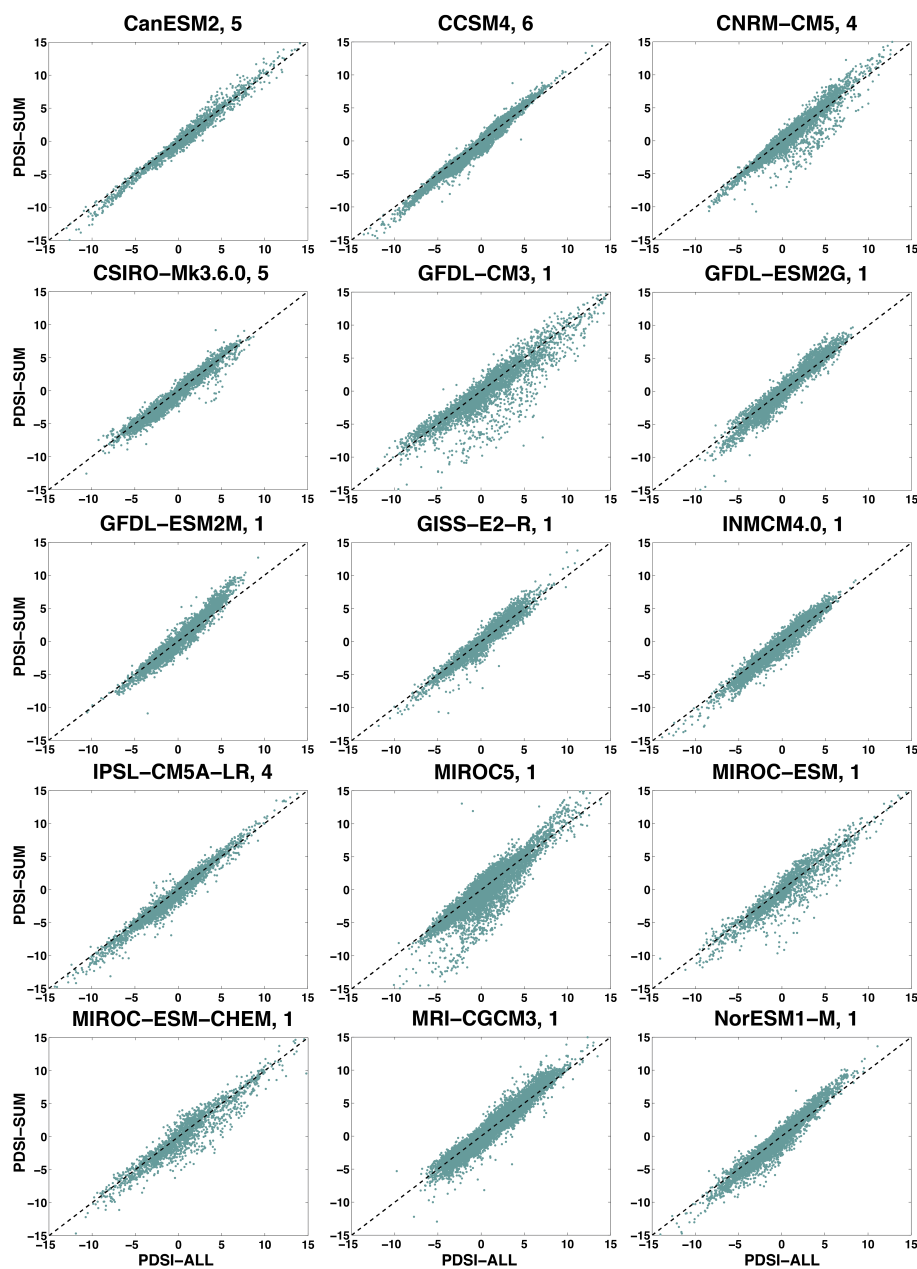


**Fig. 3** Grid cell comparisons between ensemble averaged annual PDSI (PDSI-ALL) and PDSI-SUM (PDSI-PRE + PDSI-ET) from 2080-2099 for each model in the ensemble. The dashed line indicates the 1:1 line. For those models with multiple ensemble members, the comparison is based on the ensemble average. PDSI-SUM scales linearly with PDSI-ALL, close to the 1:1 line, with some minor amplification of extreme wet or dry values in PDSI-SUM. This suggests that PDSI-ALL is well approximated as a linear sum of the pseudo-independent effects of precipitation and evapotranspiration.

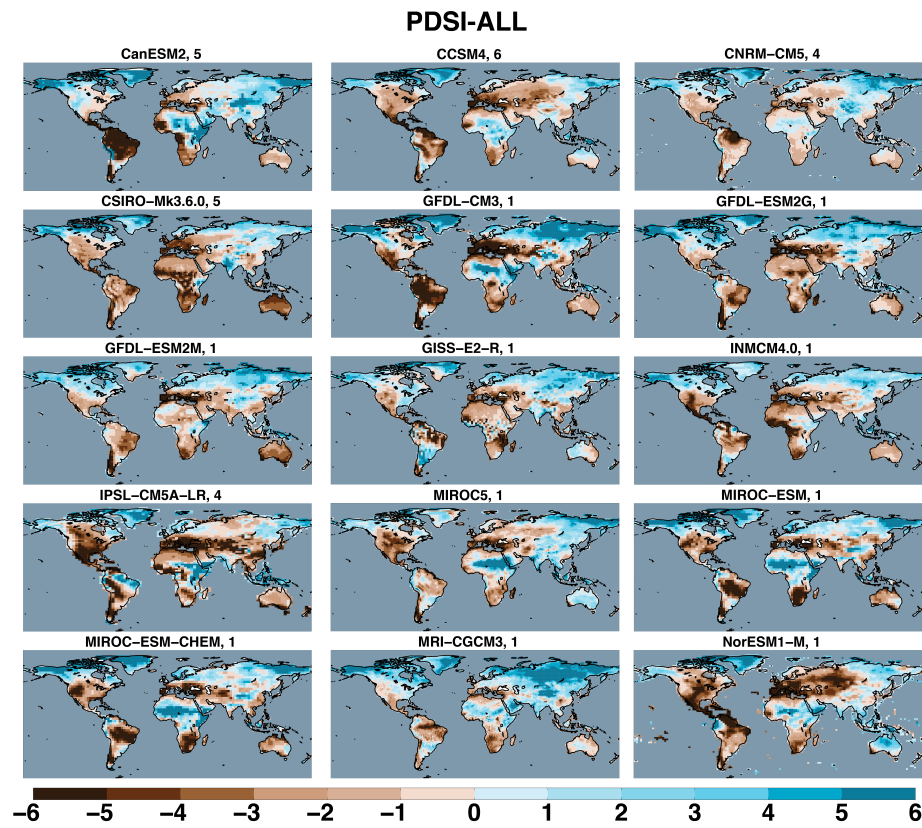
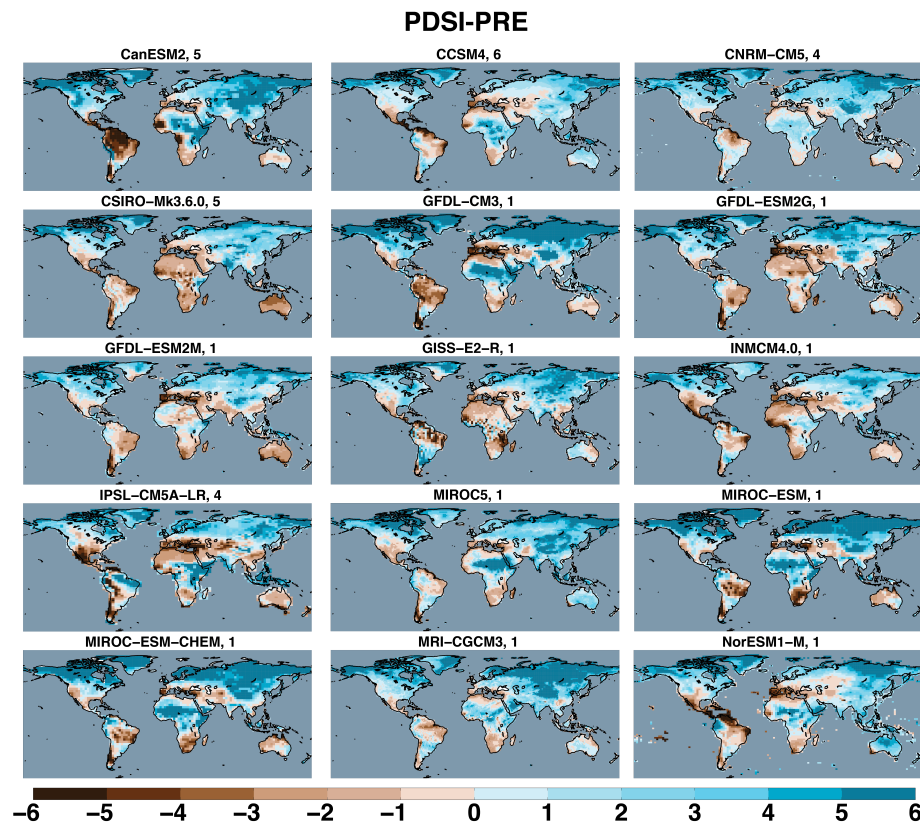
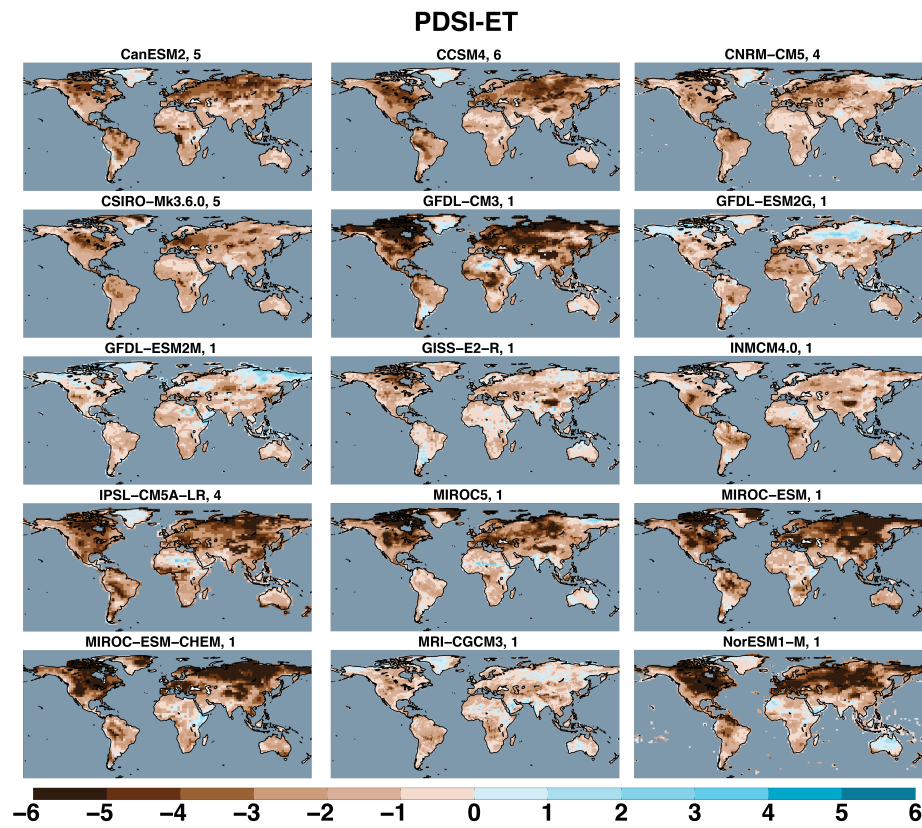


Fig. 4 Annual averaged PDSI-ALL from 2080–2099 for each model simulation under the RCP8.5 scenario. The number of ensemble members is listed in each panel title; for models with multiple ensemble members, the maps represent the ensemble average.



**Fig. 5** Annual averaged PDSI-PRE (precipitation effects only) for each model simulation under the RCP8.5 scenario. The number of ensemble members is listed in each panel title; for models with multiple ensemble members, the maps represent the ensemble average.



**Fig. 6** Annual averaged PDSI-ET (precipitation effects only) for each model simulation under the RCP8.5 scenario. The number of ensemble members is listed in each panel title; for models with multiple ensemble members, the maps represent the ensemble average.

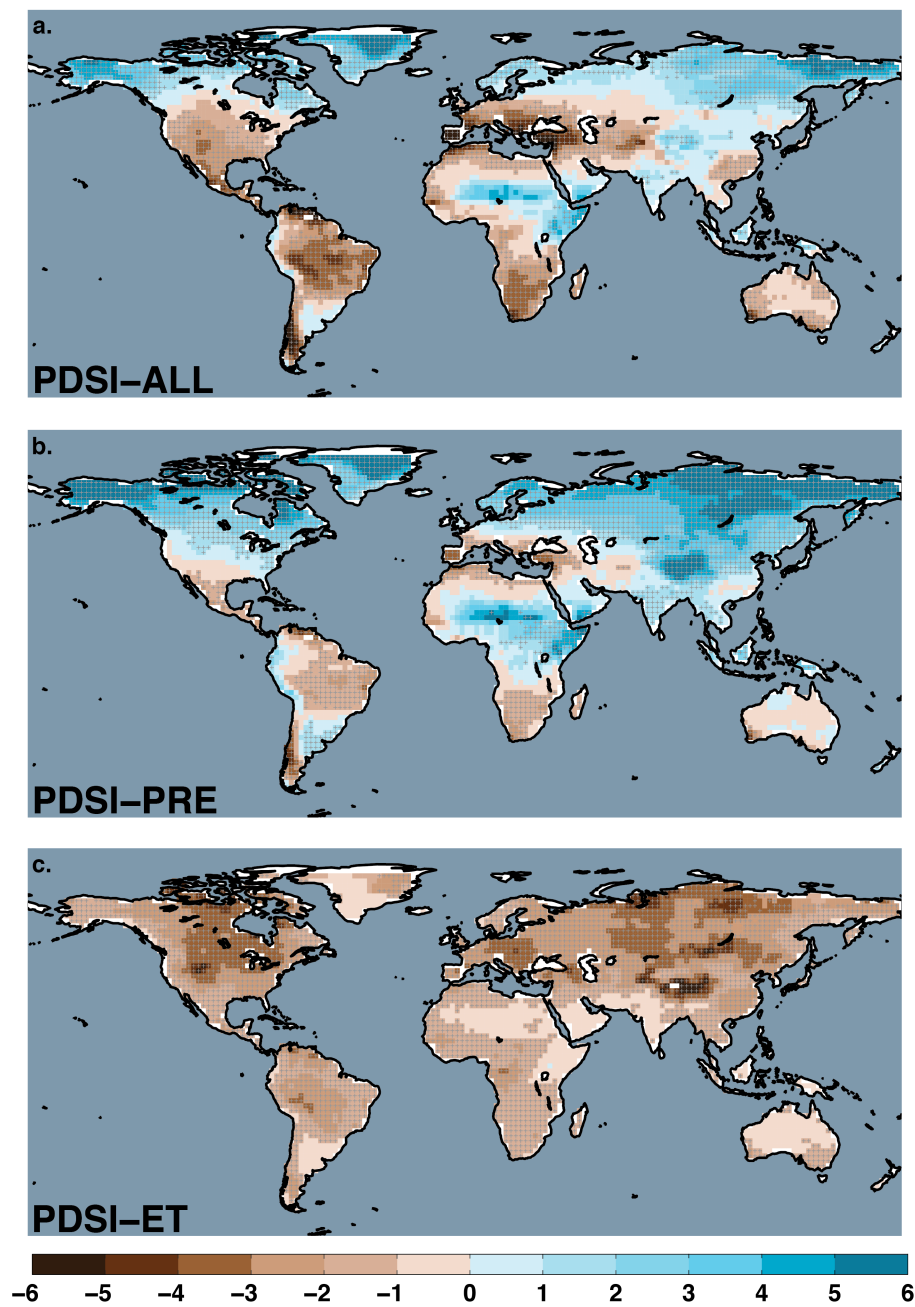


**Fig. 7** Multi-model mean PDSI for 2080-2099, for each PDSI calculation: a) PDSI-ALL, b) PDSI-PRE, and c) PDSI-ET. Cross hatching indicates cells where, for multi-model mean PDSI anomalies exceeding -1 or +1, at least 12 of the 15 models (80%) also exceed these thresholds.

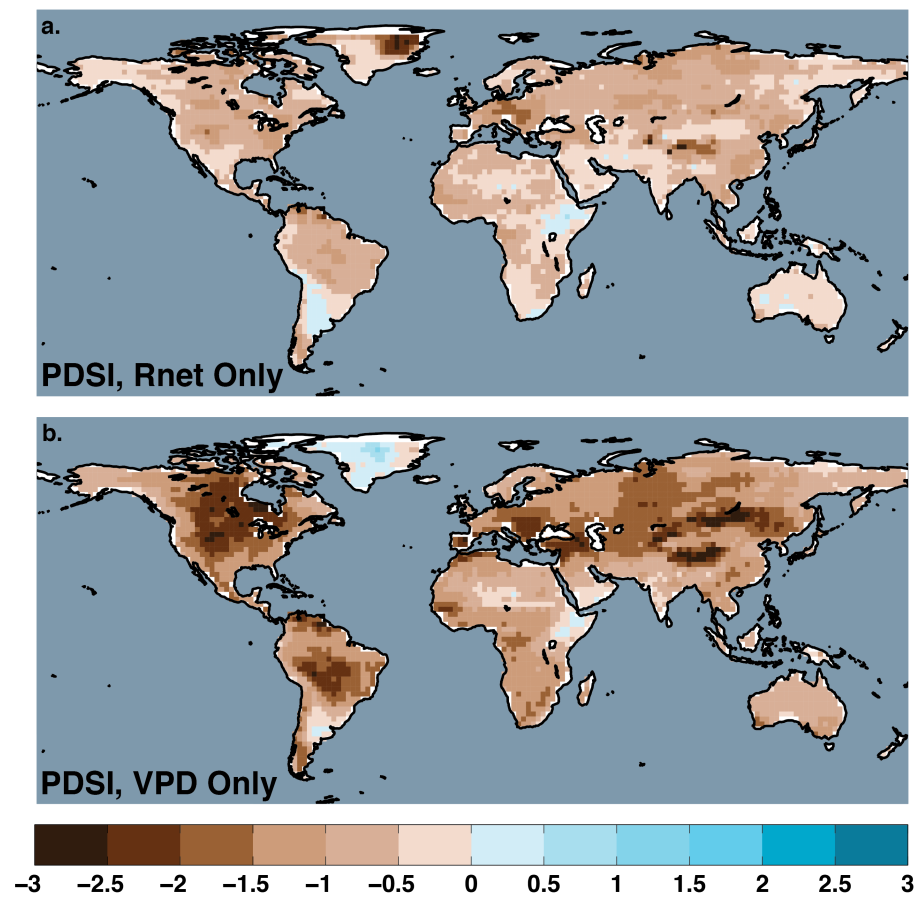


**Fig. 8** Multi-model mean PDSI projections for 2080-2090, incorporating only trends in a) surface net radiation and b) vapor pressure deficit. Note the range of values on the colorbar is half (-3 to +3) that compared to other PDSI maps, in order to better illustrate the changes.

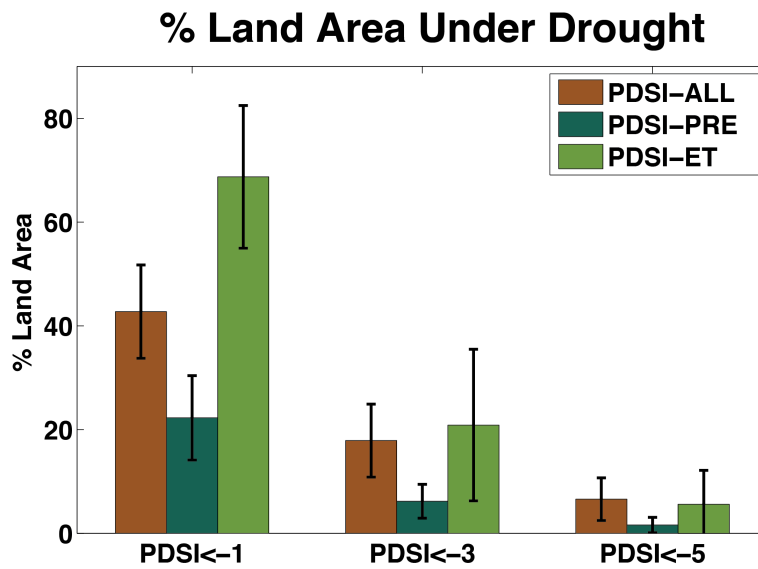


**Fig. 9** Percent land area (excluding Antarctica) with mean PDSI values (2080-2099) less than or equal to -1, -3, and -5. Bars represent the multi-model mean, and the error bars are the  $\pm 1$  standard deviation calculated across models. For models with multiple ensemble members, the ensemble average is calculated first and then used for the multi-model statistics.

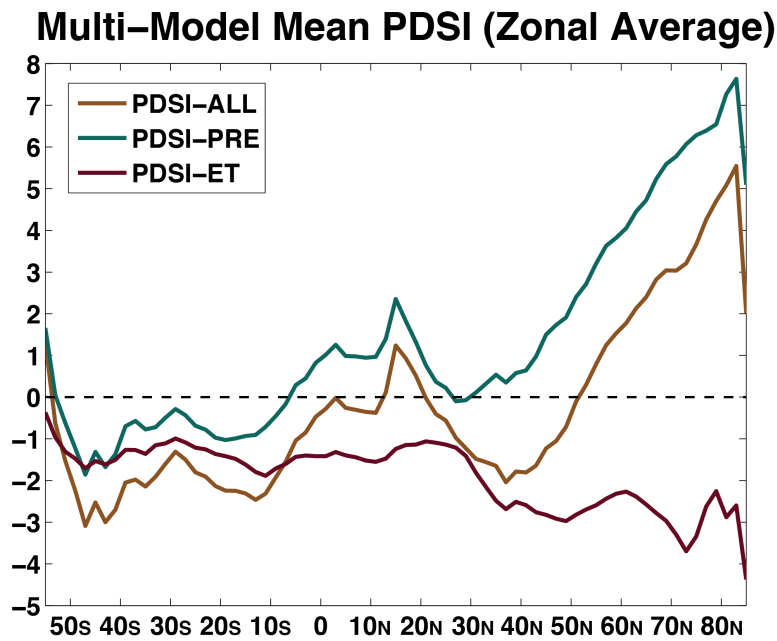


**Fig. 10** Zonally averaged multi-model mean PDSI from 2080-2099.

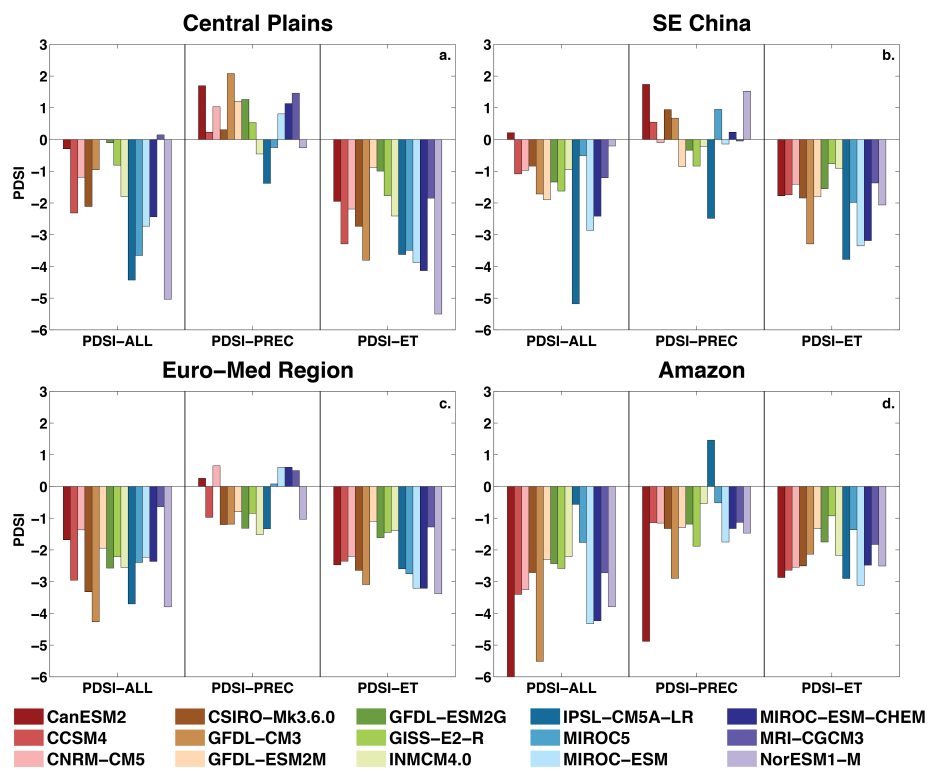


**Fig. 11** Regionally averaged PDSI for each model, over a) the central plains of North America (105°W-90°W, 32°N-50°N), b) southeast China (102°E-123°E, 22°N-30°N), c) the European-Mediterranean region (20°W-50°E, 28°N-60°N), and d) the Amazon (70°W-45°W, 20°S-5°N).